The Plant Cell, Vol. 26: 3403–3415, August 2014, www.plantcell.org

The ABC Transporter ABCG1 Is Required for Suberin Formation in Potato Tuber Periderm[W]

Ramona Landgraf,[a] Ulrike Smolka,[a] Simone Altmann,[a,1] Lennart Eschen-Lippold,[a] Melanie Senning,[b,2] Sophia Sonnewald,[b] Benjamin Weigel,[c] Nadezhda Frolova,[a] Nadine Strehmel,[a] Gerd Hause,[d] Dierk Scheel,[a] Christoph Böttcher,[a,3] and Sabine Rosahl[a,4]

[a] Leibniz Institute of Plant Biochemistry, Department of Stress and Developmental Biology, D-06120 Halle (Saale), Germany
[b] Friedrich Alexander University Erlangen-Nürnberg, Department of Biology, D-91058 Erlangen, Germany
[c] Leibniz Institute of Plant Biochemistry, Department of Bioorganic Chemistry, D-06120 Halle (Saale), Germany
[d] Martin Luther University Halle-Wittenberg, Biocenter, D-06120 Halle (Saale), Germany

The lipid biopolymer suberin plays a major role as a barrier both at plant-environment interfaces and in internal tissues, restricting water and nutrient transport. In potato (*Solanum tuberosum*), tuber integrity is dependent on suberized periderm. Using microarray analyses, we identified *ABCG1*, encoding an ABC transporter, as a gene responsive to the pathogen-associated molecular pattern Pep-13. Further analyses revealed that *ABCG1* is expressed in roots and tuber periderm, as well as in wounded leaves. Transgenic *ABCG1*-RNAi potato plants with downregulated expression of *ABCG1* display major alterations in both root and tuber morphology, whereas the aerial part of the *ABCG1*-RNAi plants appear normal. The tuber periderm and root exodermis show reduced suberin staining and disorganized cell layers. Metabolite analyses revealed reduction of esterified suberin components and hyperaccumulation of putative suberin precursors in the tuber periderm of RNA interference plants, suggesting that ABCG1 is required for the export of suberin components.

INTRODUCTION

Suberin is a biopolymer deposited in the cell wall to form a hydrophobic surface that protects against water loss and regulates diffusion of solutes and gases (Ranathunge et al., 2011). Typical suberin-containing tissues include the exo- and endodermis of roots as well as oak cork (*Quercus suber*) and potato tuber (*Solanum tuberosum*) periderm.

The suberin polymer consists of ester-linked ω-hydroxyacids, α,ω-dicarboxylic acids (DCAs), fatty acids, and primary alcohols with chain lengths ranging from C16 up to C32, as well as glycerol. In addition, suberin contains hydroxycinnamic acids, predominantly ferulic acid, that are cross-linked by both ester and nonester bonds (Franke and Schreiber, 2007; Pollard et al., 2008). Enzymes involved in the biosynthesis of suberin precursors have been identified primarily in *Arabidopsis thaliana*. The formation of ω-hydroxy fatty acids and, possibly, DCAs is catalyzed by CYP86A hydroxylases (Beisson et al., 2012). Acyl transferases of the BAHD superfamily transfer the acyl moiety of feruloyl-CoA to ω-hydroxy fatty acids and fatty alcohols (Molina et al., 2009), whereas glycerol-3-phosphate acyl transferases link fatty acyl moieties to glycerol (Beisson et al., 2007). In addition, long-chain acyl-CoA synthetases are postulated to activate free fatty acids by conjugation to CoA. Fatty acyl-CoA reductases and β-ketoacyl-CoA synthases catalyze the biosynthesis of fatty alcohols and very-long-chain fatty acids, respectively (Franke et al., 2009; Domergue et al., 2010).

How suberin monomers are transported through the plasma membrane into the apoplast is not known. The formation of cutin, the lipid polymer of plant cuticles, requires plasma membrane-localized ATP binding cassette (ABC) transporters (Bird et al., 2007; Panikashvili et al., 2011; Bessire et al., 2011); however, no ABC transporter involved in suberin deposition has been identified so far.

Potato tuber periderm cells have highly suberized walls. The function of tubers as storage organs necessitates mechanisms to reduce water loss. The importance of suberin as a transpiration barrier in potato tubers was illustrated in transgenic plants with defective periderm as a consequence of the downregulated expression of genes encoding the suberin biosynthetic enzymes β-ketoacyl-CoA synthase (KCS6; Serra et al., 2009a), CYP86A33 (Serra et al., 2009b), and ω-hydroxy fatty acid/fatty alcohol hydroxycinnamoyl transferase (FHT; Serra et al., 2010). Reduced levels of suberin in these plants were correlated with compromised transpiration barrier function.

Potato is the fourth most important crop plant worldwide. One of the major causes of yield loss in potato is late blight disease, caused by the oomycete *Phytophthora infestans* (Fry, 2008). The susceptible potato cultivar Désirée can be induced to mount efficient defense responses against *P. infestans* by treatment with the pathogen-associated molecular pattern (PAMP) Pep-13 (Halim

[1] Current address: University of Potsdam, Institute of Biochemistry and Biology, Karl-Liebknecht-Str. 24-25, 14476 Potsdam, Germany.
[2] Current address: ETH Zurich, Department of Biology, Plant Biotechnology, Universitaetstrasse 2, CH-8092 Zurich, Switzerland.
[3] Current address: Julius Kühn-Institut, Bundesforschungsinstitut für Kulturpflanzen, Institut für ökologische Chemie, Pflanzenanalytik, und Vorratsschutz, Königin-Luise-Str.19, 14195 Berlin, Germany.
[4] Address correspondence to srosahl@ipb-halle.de.
The author responsible for distribution of materials integral to the findings presented in this article in accordance with the policy described in the Instructions for Authors (www.plantcell.org) is: Sabine Rosahl (srosahl@ipb-halle.de).
[W] Online version contains Web-only data.
www.plantcell.org/cgi/doi/10.1105/tpc.114.124776

et al., 2004), ultimately conferring enhanced resistance to the whole plant. Upon infiltration into potato leaves, Pep-13, a 13-amino acid motif from an extracellular transglutaminase from *Phytophthora* species (Brunner et al., 2002; Halim et al., 2004), induces defense responses in a salicylic acid- and jasmonic acid-dependent manner (Halim et al., 2009).

As part of our functional analysis of genes that are activated in potato in response to Pep-13 infiltration, we identified a gene predicted to encode the ABC half transporter ABCG1. Analysis of plants with reduced *ABCG1* expression indicates a role for ABCG1 in suberin formation of potato tuber periderm and, thus, in water barrier formation.

RESULTS

Identification of the Pep-13-Activated *ABCG1* Gene

Susceptible potato plants (*S. tuberosum* cv Désirée) display enhanced resistance against *P. infestans* after infiltration of the PAMP Pep-13 (Halim et al., 2009). To identify genes that are activated in response to Pep-13 treatment, microarray experiments were performed using POCI oligo arrays (Kloosterman et al., 2008). RNA was isolated from leaves of potato plants after infiltration with Pep-13 or its inactive analog W2A (Brunner et al., 2002). More than 700 genes were identified as at least 2-fold upregulated by Pep-13 in wild-type plants compared with W2A treatment. An EST encoding a putative ABC half transporter (ABCG1) was chosen for further characterization (Supplemental Figure 1A). The corresponding gene was identified from the potato genome database (Xu et al., 2011; XM_006345853.1; http://www.ncbi.nlm.nih.gov/). Only one *ABCG1* gene is present in the reference genome of *S. tuberosum* group *phureja*. The coding region consists of two exons separated by an intron of 97 bp (Supplemental Figures 1C and 1D). The encoded protein of 750 amino acids is predicted to be an ABC half transporter with a P-loop-containing ATP hydrolase region and six transmembrane domains (Supplemental Figure 1E). The amino acid sequence of ABCG1 was compared with that of the 43 members of the *Arabidopsis* AtABCG family (www.arabidopsis.org). Phylogenetic analyses revealed highest homology of St-ABCG1 to At-ABCG1 and At-ABCG16 (Supplemental Figure 2 and Supplemental Data Set 1).

Expression of *ABCG1* in Potato

To verify the Pep-13-inducible expression of *ABCG1* observed in the microarrays (Supplemental Figure 1A), RNA from leaves of Pep-13-treated wild type and empty vector-containing potato plants was subjected to quantitative RT-PCR analysis. In wild-type and empty vector-carrying plants, Pep-13, but not W2A, induced the accumulation of *ABCG1* transcripts (Supplemental Figure 1A). Moreover, *ABCG1* expression was induced by wounding (Supplemental Figure 1B).

The tissue-specific expression of *ABCG1* was determined using RNA from untreated soil-grown plants. Expression was hardly detectable in leaves and stems, whereas higher levels of *ABCG1* transcripts were found in roots and in tubers (Figure 1A). Separation of tuber skin and tuber cortex revealed higher levels of *ABCG1* transcripts in tuber skin (Figure 1B).

ABCG1 Is Localized to the Plasma Membrane

The full-length coding region of *ABCG1* was amplified from cDNA reverse transcribed from RNA of Pep-13-treated potato leaves and cloned under the control of the *ubiquitin 10* promoter in front of the coding region of red fluorescent protein (RFP) in the binary vector *pUBC-DEST-RFP* (Grefen et al., 2010). Transient expression of the construct in *Arabidopsis* mesophyll protoplasts revealed RFP fluorescence at the cell periphery (Figure 2). Colocalization with the established plasma membrane marker FLS2-YFP (Robatzek et al., 2006) suggested that St-ABCG1 is plasma membrane localized.

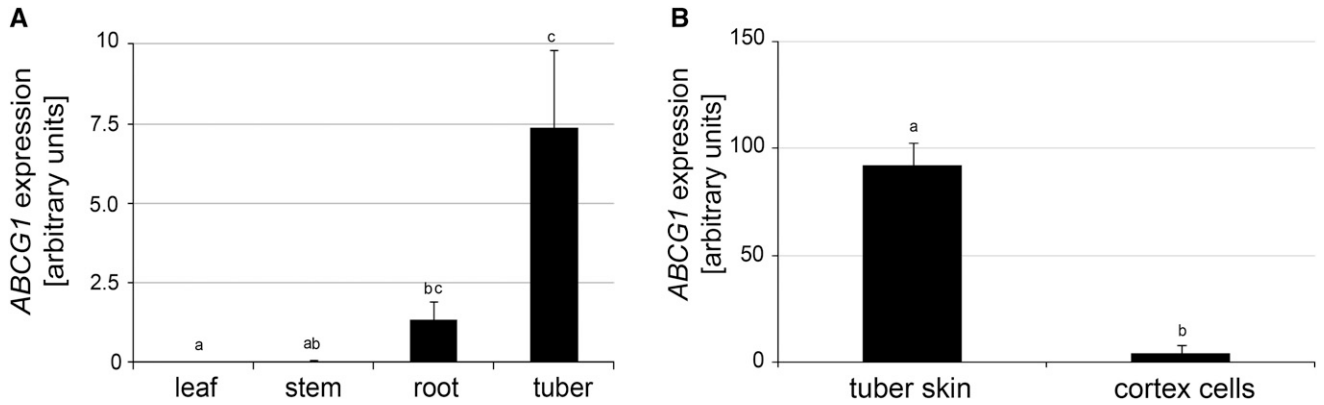

Figure 1. *ABCG1* Is Expressed in Roots and Tubers.

(A) Tissue-specific expression of *ABCG1*. RNA was isolated from leaves, stems, roots, and tubers of 5-week-old potato plants grown in a phytochamber, reverse transcribed, and analyzed for *ABCG1* transcript levels by quantitative PCR. Expression of *EF1*α was used as a reference.
(B) Expression of *ABCG1* in tubers. RNA was isolated from tuber skin and tuber cortex of 3-month-old greenhouse-grown potato plants.
Data are derived from three (**[A]**; $n = 6$) and two (**[B]**; $n = 8$) independent experiments. Error bars represent SE. Letters indicate statistically different values (one-way ANOVA, $P \leq 0.05$ **[A]** and t test, $P \leq 0.01$ **[B]**).

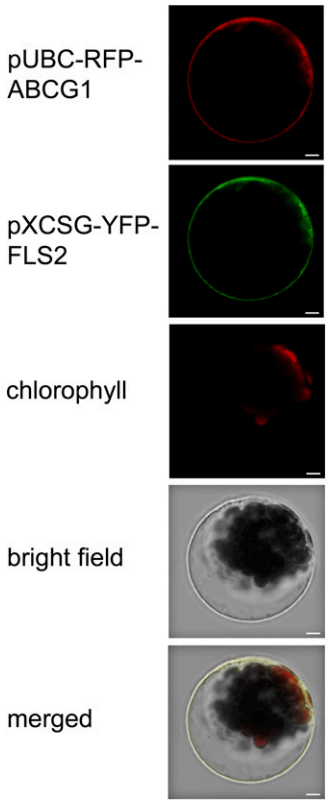

Figure 2. St-ABCG1 Colocalizes with a Plasma Membrane Protein.

Arabidopsis protoplasts were cotransfected with St-*ABCG1-RFP* and At-*FLS2-YFP*. Expression of the proteins was detected by confocal laser scanning microscopy. The channels for RFP, YFP, and chlorophyll fluorescence are shown, as well as the bright-field and merged images. The experiment was performed twice with similar results. Bars = 5 μm.

Potato Plants with Reduced Expression of *ABCG1*

To address the function of ABCG1, a 413-bp fragment, covering 210 bp of the end of the first exon and 203 bp of the second exon (Supplemental Figure 1D) was amplified from potato cDNA and cloned into *pHellsgate8* (Wesley et al., 2001). Potato plants expressing the RNA interference (RNAi) construct were generated by *Agrobacterium tumefaciens*–mediated leaf disk transformation. Twenty independent transformants were regenerated in two independent transformation experiments. Sixteen of these lines showed a reduction in wound-induced *ABCG1* expression in leaves (Supplemental Figure 3A). Moreover, *ABCG1* expression was reduced in roots (Figure 3A). The four representative lines (B4, F2, N, and P) that were tested demonstrated reduced expression in tuber skin (Figure 3B; for individual lines, see Supplemental Figure 3B).

Both roots and tubers of the RNAi plants, but not the aerial parts, displayed altered morphology (Figure 4). Notably, the tuber skin was rough, corky, and brownish, in contrast to the smooth and reddish tuber skin of wild-type plants (Figure 4A). Microscopy analyses of the tuber sections revealed morphological defects of the tuber skin of *ABCG1*-RNAi plants, possibly caused by the collapse of periderm cells. This was visualized in toluidine blue-stained tuber skin sections, revealing an altered periderm without the typical organization of stacked phellem cells (Figure 4A; for individual lines, see Supplemental Figure 4A). Due to the collapsed cells and ruptured tissue, determination of cell size and number was not possible.

The root system of soil-grown *ABCG1*-RNAi plants was less developed than that of wild-type plants and sections of roots in the root hair zone showed major defects in the outer layers (Figure 4B). Within the individual *ABCG1*-RNAi lines, these defects ranged from collapsed individual exodermal cells to completely ruptured outer cell layers (Supplemental Figure 4B). In contrast to the endodermis of wild-type roots, multiple cell layers were present around the central cylinder in the *ABCG1*-RNAi lines (Supplemental Figure 4B). As the tuber periderm and the root exodermis are tissues with suberized cell walls, fluorol yellow staining for aliphatic suberin was performed. Compared with wild-type plants, a reduction in fluorol yellow staining of cell walls was observed for both tuber periderm (Figure 4C) and the root exodermis of *ABCG1*-RNAi plants (Figure 4D). In contrast to the one-layered wild-type endodermis, *ABCG1*-RNAi plants had multiple layers of cells around the central cylinder whose walls were stained with fluorol yellow. In the same tissues, autofluorescence was stronger than in wild-type tissue (Figures 4C and 4D), suggesting an increase in phenolic compounds. Thus, the reduction in *ABCG1* expression was accompanied by reduced suberin depositions in tubers and roots.

In accordance with the reduced suberization of the periderm, *ABCG1*-RNAi tubers suffered a severe water loss during 20 d of storage, resulting in a 2-fold weight reduction, whereas control tubers did not lose weight to a significant extent (Figure 4E).

ABCG1 Downregulation Reduces the Major and Alters the Profile of Minor Monomers of Aliphatic Tuber Suberin

To elucidate the effect of *ABCG1* downregulation on the monomer composition of the esterified part of suberin, tuber periderm of *ABCG1*-RNAi and control (wild-type and empty vector) plants was digested with cell wall-degrading enzymes, delipidated, and depolymerized by acid-catalyzed methanolysis. After trimethylsilylation, released monomers were relatively quantified by gas chromatography-mass spectrometry (GC-MS) (Supplemental Tables 1 to 4). *ABCG1*-RNAi periderm had strongly reduced levels of the major aliphatic monomers ω-hydroxy-octadec-9-enoic acid (ω-OH-C18:1) and octadec-9-enedioic acid (α,ω-DCA-C18:1), which accumulated on average to 9 and 18% of the control periderm level, respectively (Figures 5A and 5B). Within the four investigated RNAi lines, the range of monomer accumulation was 2 to 16% (ω-OH-C18:1) and 3 to 33% (α,ω-DCA-C18:1) of control periderm levels (Supplemental Figures 5A and 5B). Among the minor monomers, ω-hydroxy fatty acids, fatty acids, and fatty alcohols of chain-length C24, C26, C28, and C30 showed a similar strong reduction in *ABCG1*-RNAi periderm compared with control periderm as that observed for the two major monomers (Figures 5A, 5C, and 5D). By contrast, *ABCG1* downregulation was correlated with significantly higher amounts of saturated ω-hydroxy fatty acids, α,ω-dicarboxylic acids, and fatty acids of chain lengths of C16 to C22 (Figures 5A to 5C). In addition, less ferulic acid was released after methanolysis of tuber periderm from *ABCG1*-RNAi plants compared with control periderm (Figure 5E).

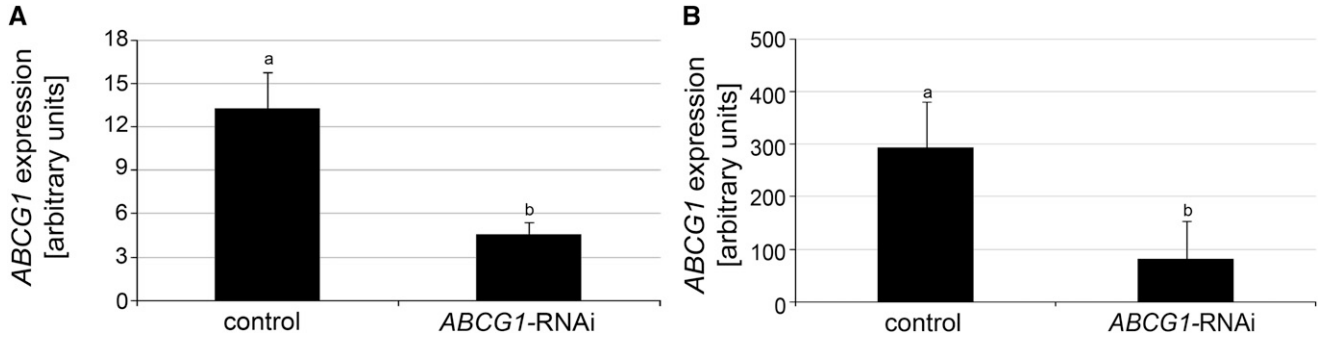

Figure 3. *ABCG1* Expression Is Reduced in *ABCG1*-RNAi Lines.

(A) Reduced *ABCG1* expression in roots of *ABCG1*-RNAi lines. Quantitative RT-PCR analysis of RNA isolated from untreated roots of 3-week-old wild-type and empty vector plants ("control") and *ABCG1*-RNAi plants (lines A, B4, F2, and K) grown in a phytochamber. Expression of *EF1*α was used as a reference. Data are derived from three independent experiments (n = 18). Error bars represent SE. Different letters indicate statistically significant differences (t test, $P \leq 0.002$).

(B) Reduced *ABCG1* expression in tuber skin of *ABCG1*-RNAi lines. RNA was isolated from tuber skin of 3-month-old control and *ABCG1*-RNAi plants (lines B4, F2, N, and P) grown in a greenhouse. Data are derived from two independent experiments (control, n = 12; *ABCG1*-RNAi, n = 27). Different letters represent statistically significant differences (t test, $P \leq 0.001$).

ABCG1 Downregulation Is Accompanied by Accumulation of Monomeric Suberin Precursors in Tuber Periderm

To test whether the strong reduction of the majority of esterified suberin monomers upon *ABCG1* downregulation is correlated with the accumulation of monomeric suberin precursors, apolar extracts of tuber periderm were subjected to ultraperformance liquid chromatography (UPLC)/photodiode array (PDA)/electrospray ionization (ESI)-quantitative time-of-flight mass spectrometry (QTOFMS). Comparative analyses of UV chromatograms revealed numerous compounds with an absorption maximum at 324 nm and dramatically increased levels in *ABCG1*-RNAi periderm in comparison to control periderm (Supplemental Figure 6). Among them, a homologous series of feruloyloxy fatty acids with chain lengths of C16 to C28 was identified by combined analysis of accurate mass, isotope pattern, and collision-induced dissociation (CID) mass spectra (Supplemental Figure 7 and Supplemental Table 5). Although the acquired CID mass spectra do not allow deduction of the position of the feruloyloxy moiety nor the branching pattern of the alkyl chain, it is likely that these components represent straight-chain ω-feruloyloxy fatty acids. In addition, a derived homologous series of C16-C28 feruloyloxy fatty acids esterified with glycerol was identified from *ABCG1*-RNAi periderm extracts (Supplemental Table 6). In contrast to feruloyloxy fatty acids, which give rise to two chromatographically separable peaks due to the presence of (*E*)- and (*Z*)-configured feruloyloxy moieties, four chromatographic peaks could be resolved for individual feruloyloxy fatty acid glycerol esters (Supplemental Figure 8). This suggests that both 1-/3-*O*- and 2-*O*-(feruloyloxy alkanoyl) glycerols are present in the extract. Assuming equal response factors, the homolog profiles of feruloyloxy fatty acids and derived glycerol esters show a maximum abundance at a chain length of C22.

Besides feruloyloxy fatty acids and their glycerol esters, numerous other ferulic acid conjugates could be detected on the basis of their UV absorption and characterized by ESI-QTOFMS as alkyl ferulates (chain length C16-C28), hydroxyalkyl ferulates (chain length C18-C24), and feruloyloxyalkyl ferulates (chain length C16-C24; Supplemental Tables 7 to 9). Relative quantification of these components revealed increased levels of hydroxyalkyl ferulates, except for chain length C21, and feruloyloxyalkyl ferulates in *ABCG1*-RNAi periderm in relation to control periderm (Supplemental Table 10; Figure 6 for compounds with even-numbered chain length). By contrast, hyperaccumulation of alkyl ferulates in *ABCG1*-RNAi periderm in comparison to control periderm was only observed for species with chain lengths of C18, C19, C20, and C22.

The application of UPLC/PDA/ESI(-)-QTOFMS additionally facilitated relative quantification of other putative suberin precursors from apolar periderm extracts such as ω-hydroxy fatty acids, α,ω-DCAs, and fatty acids. Here, homologous series of ω-hydroxy fatty acids (chain length C20-C26) and α,ω-DCAs (chain length C20-C26) were found to accumulate to significantly higher amounts in *ABCG1*-RNAi periderm in comparison to control periderm (Figures 6F and 6G). For fatty acids, homologs with chain lengths of C16 to C24, except C18:2, had increased levels in *ABCG1*-RNAi periderm in comparison to control periderm (Figure 6H). In particular, the level of C18:1 was more than 20-fold higher in *ABCG1*-RNAi periderm than in control periderm.

StABCG1 Downregulation Induces Accumulation of Hydroxycinnamic Acid Conjugates in Tuber Periderm

To study the effect of *ABCG1* downregulation on the semipolar metabolite profile of tuber periderm, methanolic periderm extracts of *ABCG1*-RNAi and control periderm were subjected to UPLC/PDA/ESI-QTOFMS. Comparative analyses of the resulting data revealed dramatically increased levels of (hydroxy)cinnamoyl/benzoyl putrescine conjugates, dihydro hydroxycinnamoyl putrescine conjugates, and cross-linked dehydrodimers of feruloyl tyramine and feruloyl octopamine in *ABCG1*-RNAi in comparison to control periderm (Table 1). By contrast, caffeic and chlorogenic acid, the latter being the major phenolic compound detectable in control periderm, were found to be reduced in *ABCG1*-RNAi periderm to 13 and 37% of control periderm levels, respectively. In agreement with the brownish periderm of *ABCG1*-RNAi tubers, reduced levels of

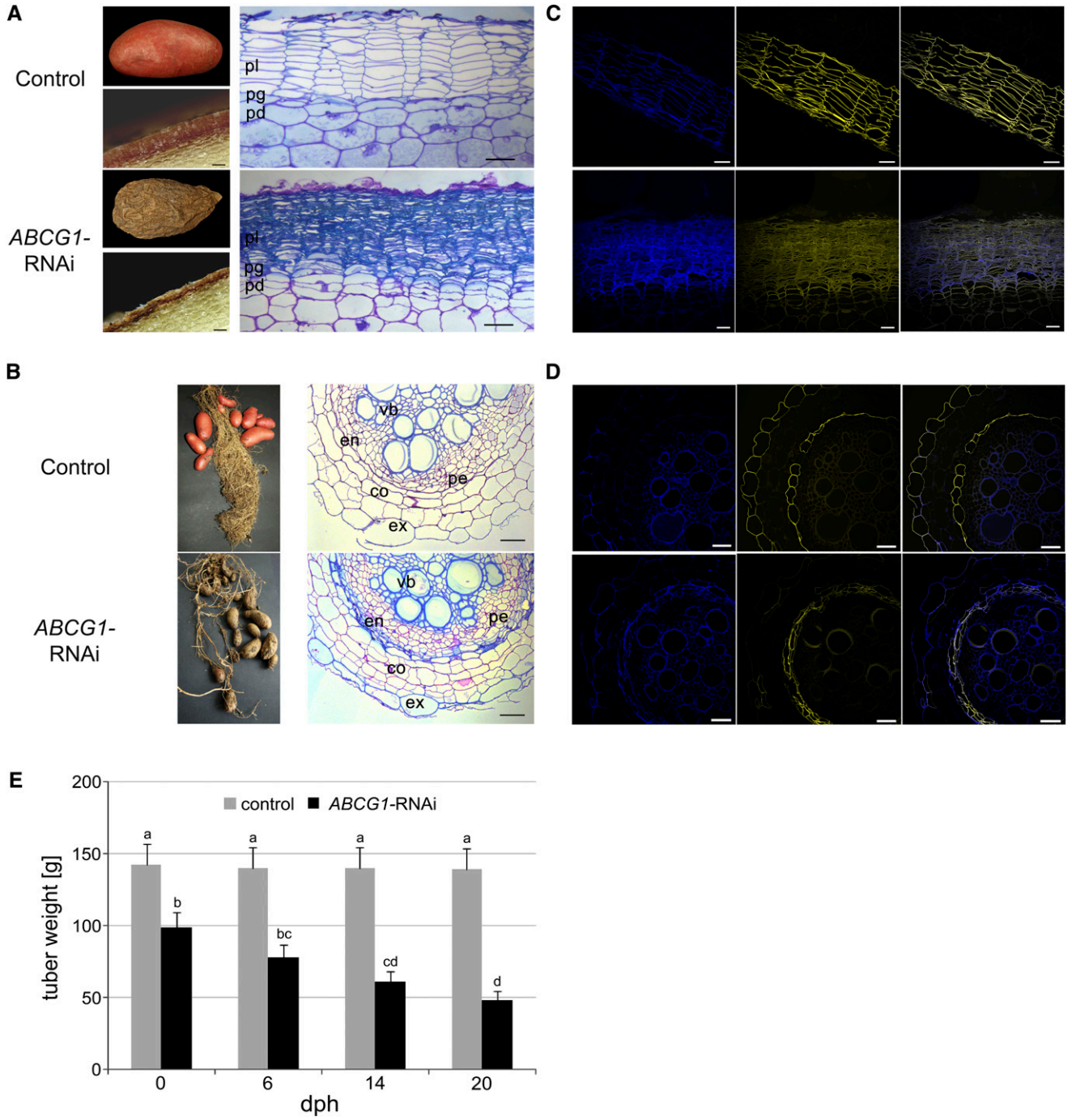

Figure 4. Morphological Alterations in *ABCG1*-RNAi Plants.

(A) Tuber phenotype of wild-type (top panel) and *ABCG1*-RNAi (bottom panel) plants. Tubers were harvested from greenhouse-grown potato plants and analyzed after 1 week of storage at 4°C (left). Microscopy of cross sections of wild-type and *ABCG1*-RNAi tubers is shown on the right. pl, phellem; pg, phellogen; pd, phelloderm. Bars = 80 μm.

(B) Root phenotype of wild-type (top panel) and *ABCG1*-RNAi (bottom panel) plants. Microscopy of cross sections of empty vector and *ABCG1*-RNAi roots is shown on the right. ex, exodermis; co, cortex; en, endodermis; vb, vascular bundle; pe, pericycle.

(C) Reduced suberin staining of tuber periderm of wild-type (top panel) and *ABCG1*-RNAi (bottom panel) plants. Cross sections of potato tuber periderm were stained with fluorol yellow and subjected to fluorescence microscopy (left, autofluorescence; middle, fluorol yellow; right, merged). Bars = 50 μm.

(D) Reduced suberin staining of the root exodermis of wild-type (top panel) and *ABCG1*-RNAi (bottom panel) plants. Cross sections of roots were stained with fluorol yellow and subjected to fluorescence microscopy (left, autofluorescence; middle, fluorol yellow; right, merged). Bars = 50 μm.

(E) Tuber weight loss of *ABCG1*-RNAi plants. Tubers were harvested from greenhouse-grown control (gray bars) and *ABCG1*-RNAi plants (black bars) and stored at room temperature. Tuber weight was determined at the time points indicated (n = 41, three independent experiments, two independent RNAi lines, days postharvest [dph]). Error bars represent SE. Letters indicate statistically different values (two-way ANOVA, $^{b}P \leq 0.05$, $^{c,d}P \leq 0.01$).

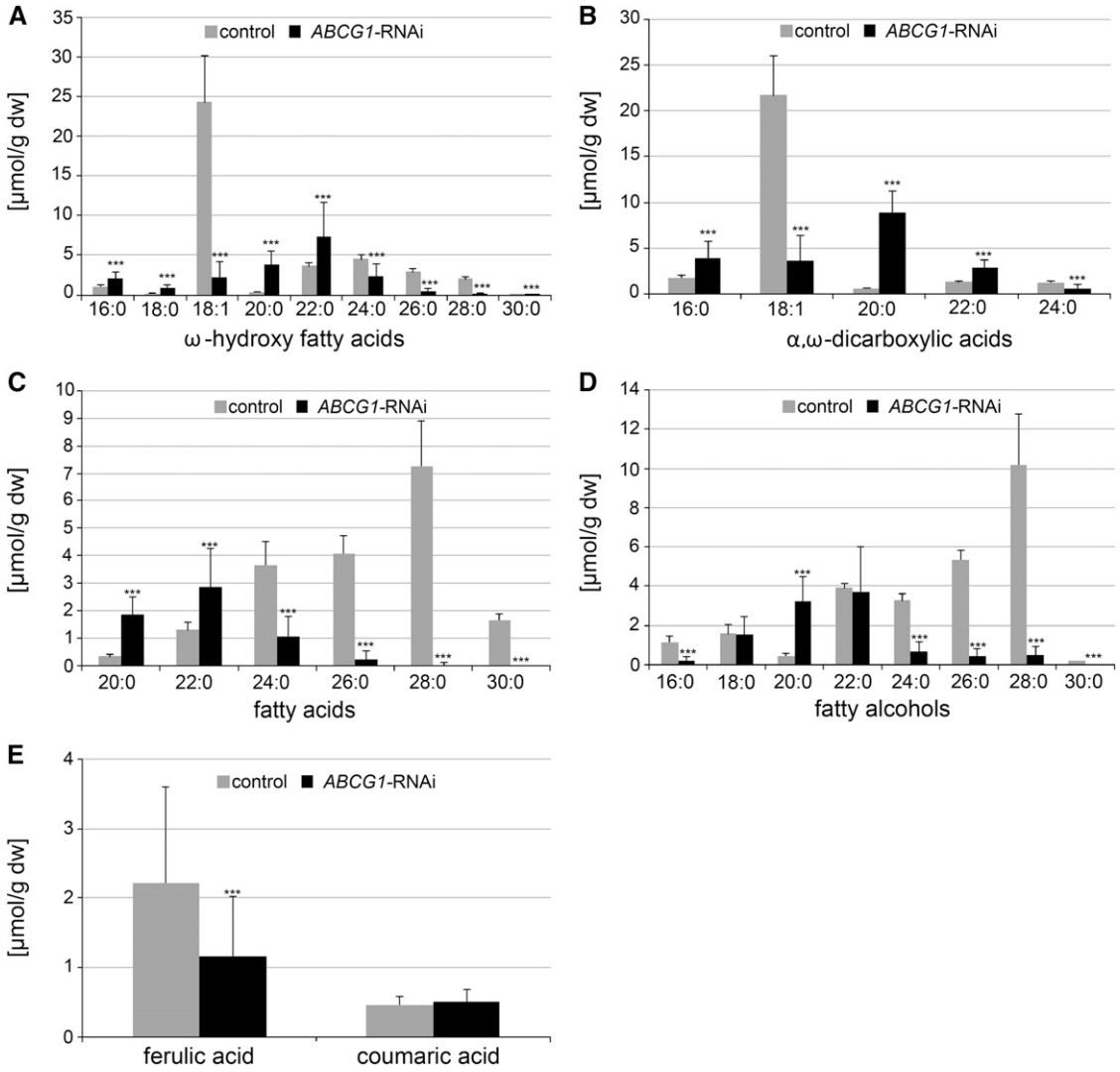

Figure 5. Monomer Composition of Aliphatic Suberin of Control and *ABCG1*-RNAi Tuber Periderm.

Digested and delipidated periderm disks of *ABCG1*-RNAi (four independent lines: $n = 32$) and control (wild type: $n = 8$, empty vector: $n = 8$) tubers from two independent experiments were depolymerized and released monomers analyzed by GC-MS. Monomers were quantified using quantifier ions/retention times from Supplemental Tables 1 to 4 and 15. Values shown represent medians ± SD. Significance analysis of differences between *ABCG1*-RNAi and control was performed by *t* test (two-tailed, unequal variances): ***$P \leq 0.001$.

anthocyanins, accounting for the reddish pigmentation of the control periderm, were detected in *ABCG1*-RNAi in relation to control periderm. Changes in the accumulation of the major glycoalkaloids, α-solanine, and α-chaconine were less pronounced between *ABCG1*-RNAi and control periderm.

DISCUSSION

The ABC Half Transporter ABCG1 Is Required for Suberin Deposition

Downregulation of a PAMP-responsive gene encoding the plasma membrane-localized half transporter ABCG1 resulted in reduced suberization of the tuber periderm and root exodermis as indicated by fluorol yellow staining and GC-MS analysis. Although it cannot be ruled out that ABCG1 is involved in the transport of a factor required for suberin polymerization, our results are consistent with the hypothesis that ABCG1 is necessary for the export of suberin monomers. Moreover, highly decreased levels of the two major monomers, ω-OH-C18:1 and α,ω-DCA-C18:1 (Serra et al., 2010), as well as ω-hydroxy fatty acids, α,ω-DCAs, and fatty alcohols with a chain length of C24 and longer in *ABCG1*-RNAi plants (Figure 5) suggest that the loss of ABCG1 function affects the export of suberin components in a chain length-specific manner.

Liquid chromatography-mass spectrometry analyses of apolar periderm extracts, comprising both intra- and extracellular lipids, revealed hyperaccumulation of several ferulic acid conjugates,

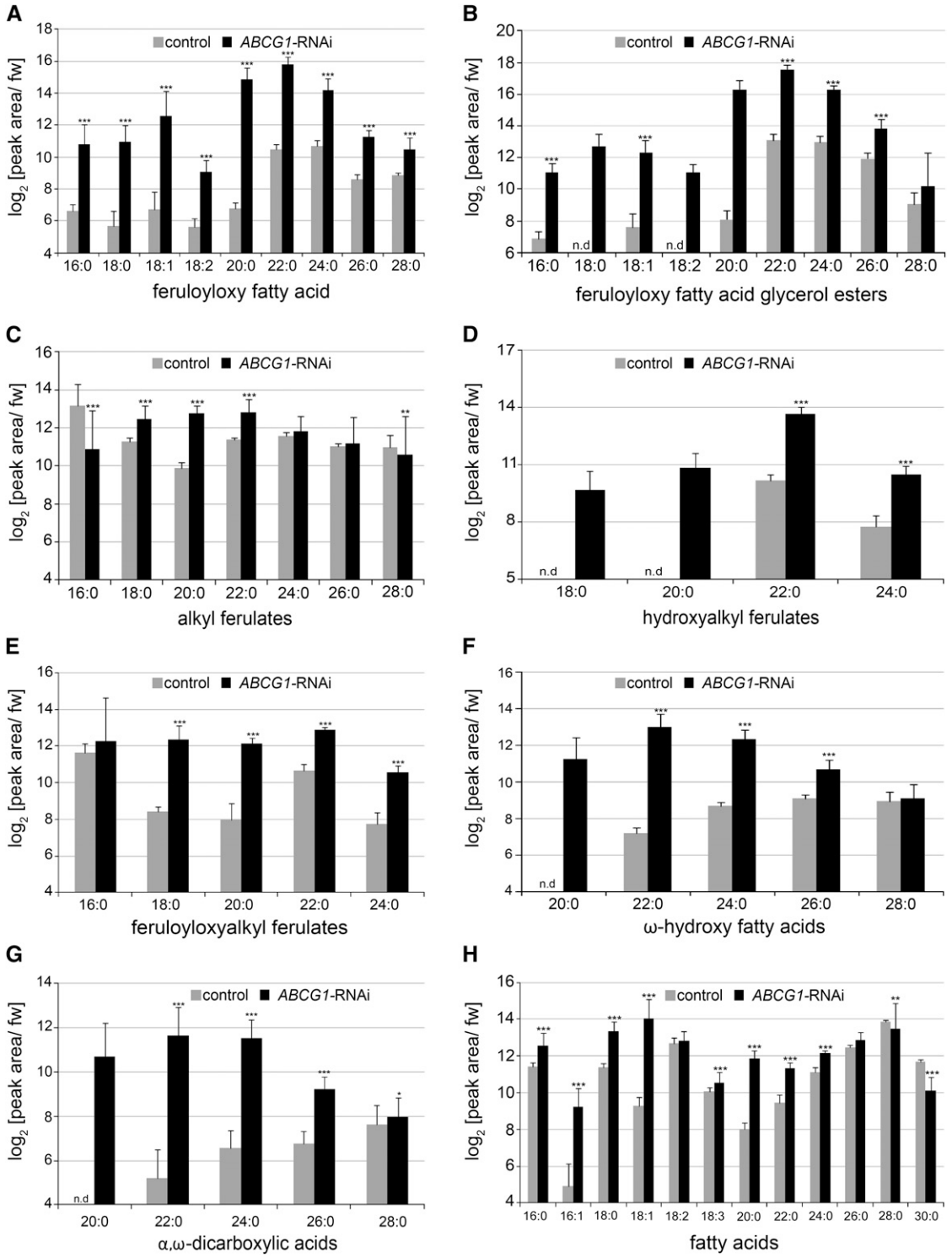

Figure 6. Relative Quantification of Ferulic Acid Conjugates, ω-Hydroxy Fatty Acids, α,ω-Dicarboxylic Acids, and Fatty Acids in Apolar Extracts of *ABCG1*-RNAi and Control Periderm.

Methyl *tert*-butyl ether extracts of *ABCG1*-RNAi (four independent lines [$n = 32$]) and control (wild type [$n = 8$], empty vector [$n = 8$]) tuber periderm were prepared and analyzed by UPLC/PDA/ESI(-)-QTOFMS. Target compounds were relatively quantified using quantifier ions/retention times from Supplemental Tables 5 to 9 and 12 to 14. Resulting peak areas were normalized to fresh weight and $\log_2$ transformed. Only compounds with even-numbered chain length are shown. Values represent medians ± SD. Significance analysis of differences between *ABCG1*-RNAi and control was performed by *t* test (two-tailed, unequal variances): *$P \leq 0.05$, **$P \leq 0.01$, and ***$P \leq 0.001$. "-" indicates that the corresponding quantifier ion was below the detection limit.

Table 1. Relative Quantification of Aromatic Amino Acids, Phenolics, Anthocyanins, and Glycoalkaloids in Semi-Polar Extracts of *ABCG1*-RNAi and Control Periderm

	Log_2(Peak Area/Fresh Weight) Median ± SD	
Compound	Control	*ABCG1*-RNAi
Phe	11.9 ± 0.5	9.9 ± 0.8***
Tyr	12.5 ± 0.4	11.7 ± 1.0***
Trp	11.8 ± 0.4	11.4 ± 1.1
Caffeic acid	9.6 ± 0.9	6.7 ± 1.6***
Chlorogenic acid	14.2 ± 0.3	12.8 ± 0.6***
Cinnamoyl putrescine	n.d.	9.5 ± 1.3
Coumaroyl putrescine	n.d.	10.9 ± 1.5
Caffeoyl putrescine	7.4 ± 0.5	14.4 ± 1.4***
Dihydrocaffeoyl putrescine	7.0 ± 0.7	14.3 ± 1.9***
Feruloyl putrescine	9.8 ± 0.6	14.9 ± 1.0***
Dihydroferuloyl putrescine	9.7 ± 0.6	12.2 ± 1.0***
Vanilloyl putrescine	7.7 ± 0.3	9.3 ± 0.5***
Feruloyl tyramine (FT)	9.1 ± 0.5	8.3 ± 0.9***
Feruloyl octopamine (FO)	9.0 ± 1.1	9.5 ± 1.3
FT-FT dehydrodimer	5.4 ± 0.8	12.7 ± 0.8***
FT-FO dehydrodimer	n.d.	10.4 ± 1.0
Pelargonidin-3-(coumaroyl-Rha-Glc)-5-Glc	11.3 ± 0.9	9.5 ± 2.0***
Pelargonidin-3-(feruloyl-Rha-Glc)-5-Glc	9.7 ± 0.7	8.4 ± 2.0***
α-Chaconine	13.6 ± 0.3	13.2 ± 1.2**
α-Solanine	10.6 ± 0.4	10.2 ± 1.0**

Methanolic extracts of *ABCG1*-RNAi (line N [$n = 8$], line P [$n = 8$], line B [$n = 8$], line F [$n = 8$]) and control (wild type [$n = 8$] and empty vector [$n = 8$]) tuber periderm were prepared and analyzed by UPLC/PDA/ESI(+)-QTOFMS. Target compounds were relatively quantified using quantifier ions/retention times from Supplemental Table 11. Resulting peak areas were normalized to fresh weight and log_2 transformed. Values shown represent medians ± SD. Significance analysis of differences between *ABCG1*-RNAi and control was performed by *t* test (two-tailed, unequal variances): *P ≤ 0.05, **P ≤ 0.01, and ***P ≤ 0.001. n.d., not detectable.

ω-hydroxy fatty acids, α,ω-DCAs, and fatty acids in *ABCG1*-RNAi periderm. Besides alkyl ferulates and fatty acids, which are known components of suberin-associated waxes (Schreiber et al., 2005; Serra et al., 2009b, 2010), the detected components could represent nonpolymerized suberin monomers, related precursors, or degradation products.

Interestingly, the reduction of polymerized C18:1 species and aliphatic species with chain lengths of C24 or longer in *ABCG1*-RNAi suberin (Figure 5) is not reflected by a concomitant increase of corresponding nonpolymerized molecular species in the apolar periderm fraction. This observation is in accordance with the hypothesis that downregulation of the ABCG1-mediated transport process leads to a backup of suberin monomers and their precursors inside the cell, thereby disturbing the whole monomer biosynthetic network by feedback inhibition. Consequently, homolog profiles of the monomers in wild-type polymer and in *ABCG1*-RNAi periderm extracts differ dramatically. The underrepresentation of ω-OH-C18:1 conjugates and α,ω-DCA-C18:1 in apolar *ABCG1*-RNAi periderm thereby seems to be partly compensated for by highly increased levels of the precursor fatty acid C18:1.

Putative Substrates of ABCG1

Due to the difficulty of direct transport assays (Bird et al., 2007; Bessire et al., 2011), the compounds transported by ABCG1 have not been identified. The specific reduction in suberin monomers with a chain length of C24 and longer, in addition to the reduction of the major compounds ω-OH-C18:1 and α,ω-DCA-C18:1, suggests an ABCG1-dependent export of these compounds. For cutin, the export of 2-monoacylglycerols (2-MAGs) and their extracellular polymerization by the cutin synthase CD1, a GDSL family protein, has been reported (Yeats et al., 2012). 2-MAGs are synthesized by the *sn*-2-specific glycerol-3-phosphate acyltransferases GPAT4 and GPAT6 (Li et al., 2007b; Yang et al., 2010). Overexpression of GPAT5 in *Arabidopsis* resulted in enhanced levels of MAGs in cuticular waxes, suggesting that the product of the GPAT5-mediated reaction is exported (Li et al., 2007a). Assuming that suberin formation involves comparable mechanisms to the biosynthesis of cutin, ABCG1 might be involved in the transport of compounds similar to 2-MAGs which would subsequently be polymerized by CD1-equivalent enzymes. As suberin contains ferulic acid, in contrast to cutin, the conspicuous increase in ω-feruloyloxy fatty acid glycerol esters in transport-deficient *ABCG1*-RNAi plants (Figure 6B) might suggest that these MAG derivatives are normally transported in an ABCG1-dependent process. In support of this notion, the loss of FHT function results in decreased levels of ω-OH-C18:1, one of the major components of potato tuber suberin (Serra et al., 2010). FHT catalyzes the formation of ω-feruloyloxypalmitic acid in vitro (Serra et al., 2010) and is possibly involved in the formation of ω-feruloyloxy fatty acids and, thus, ω-feruloyloxy fatty acid glycerol esters in vivo. The decreased levels of ω-OH-C18:1 in suberin in *FHT*-RNAi plants suggests that ω-OH-C18:1 is transported out of the cell after conjugation to ferulic acid. Interestingly, the levels of α,ω-DCA-C18:1 are not reduced in *FHT*-RNAi plants (Serra et al., 2010), suggesting that ferulic acid is not required for the export of this compound. Moreover, compromised formation of hydroxylated fatty acids and DCA in transgenic potato plants with reduced expression of *CYP86A33*, the potato ortholog of the *Arabidopsis* fatty acid ω-hydroxylase gene *CYP86A1* (Benveniste et al., 1998; Höfer et al., 2008), correlates with a 60% reduction in glycerol levels in suberin of tuber periderm (Serra et al., 2009b), pointing to a possible requirement of ω-hydroxylation to export glycerol.

Implications of ABCG1 Downregulation on Water Permeance and Root Morphology

The alterations in aliphatic suberin of tuber periderm of *ABCG1*-RNAi plants emphasize the importance of suberin for functional barriers. After 20 d of storage at room temperature, *ABCG1*-RNAi tubers had lost half their weight (Figure 4E), suggesting an impaired water barrier function. Water permeance has been determined for suberin-deficient tuber periderm of *KCS6*-RNAi lines, with downregulated expression of a β-ketoacyl-CoA synthase gene, and of *CYP86A33*- and *FHT*-RNAi plants, to be 1.5, 3.5, and 15 times higher than in the wild type, respectively (Serra et al., 2009a, 2009b, 2010). The highest increase in water permeance detected in *FHT*-RNAi tubers correlates with the phenotype of disorganized phellem cell layers (Serra et al., 2010).

ABCG1-RNAi tubers have a similar morphological phenotype (Figure 4A) and an even greater weight loss upon storage than *FHT*-RNAi tubers (Figure 4E; Serra et al., 2010). Thus, the absence of a functional water barrier results in the collapse of phellem cells and more brittle and fragile tuber skin (Serra et al., 2010). This is in accordance with the report that the seed coat of the *Arabidopsis gpat5* mutant is more fragile (Beisson et al., 2007).

The reduced suberin staining in the root exodermis of *ABCG1*-RNAi plants correlates with multiple layers of cells with fluorol yellow-stainable walls surrounding the central cylinder of the root (Figure 4D). Moreover, these cells show an enhanced autofluorescence. Possibly, the loss of the exodermal cell layer leads to the generation of a novel water barrier in the inner parts of the roots, consisting of both suberin and phenolic compounds.

ABCG1 Differs from *Arabidopsis* ABC Transporters Required for Cutin, Wax, and Suberin Formation

ABCG1 belongs to a different clade of ABCG transporters than the previously identified *Arabidopsis* ABCG half transporters ABCG11 (Bird et al., 2007), ABCG12 (Pighin et al., 2004), ABCG13 (Panikashvili et al., 2011), and the full transporter ABCG32 (Bessire et al., 2011) involved in the formation of cutin, waxes, and suberin components (Supplemental Figure 2). The sequence similarity of St-ABCG1 to At-ABCG11, At-ABCG12, At-ABCG13, and At-ABCG32 is 33, 31, 30, and 25%, respectively, whereas At-ABCG1 and At-ABCG16, the closest homologs, display 72 and 73% identity at the amino acid level, respectively. Only the ABC transporter At-ABCG11, required for cuticular lipid secretion (Bird et al., 2007), has been implicated in suberin formation in roots, based on the analysis of transgenic *ABCG11*-silenced plants (Panikashvili et al., 2010). Root suberin monomers analyzed from these plants contained 2-fold less C20 fatty acids, C18 fatty alcohol, ω-OH-C16, and ω-OH-C18:1, but did not show alterations in other compounds. As proposed by Panikashvili et al. (2010), the observed alteration in suberin composition in the silenced lines might be a secondary effect due to competition for common precursors of cutin and suberin. Moreover, alterations in root suberin components were not reported for *abcg11* plants. In addition, the expression pattern of *ABCG11* in root tips and lateral roots (Bird et al., 2007) does not argue for a role of ABCG11 for suberin formation.

The strong morphological phenotype observed in *ABCG1*-RNAi periderm, as well as the drastic reduction in several suberin components, therefore suggest that ABCG1 is the major ABC transporter required for suberin formation in potato tuber periderm and, possibly, in the root exodermis.

METHODS

Plant Lines and Growth Conditions

Sterile potato plants (*Solanum tuberosum* cv Désirée) were grown in tissue culture in a phytochamber under long-day conditions with 16 h light (~140 $\mu mol \cdot m^{-2} \cdot s^{-1}$) at 22°C. Potato plants were transferred to steam-sterilized soil and grown for 3 to 4 weeks in a phytochamber with 16 h light (~140 $\mu mol \cdot m^{-2} \cdot s^{-1}$) at 20°C and 60% relative humidity. Tubers were harvested from plants grown in the greenhouse for 3 months.

Treatment of Plants

PAMP treatments were performed by infiltrating a solution of 100 μM Pep-13 or the inactive analog W2A (Brunner et al., 2002) into the abaxial side of leaves of 3-week-old potato plants growing in a phytochamber. For wounding experiments, leaves were treated with a hemostat.

Expression Analyses

RNA from leaves, tubers, and roots was isolated as described (Halim et al., 2004) including a DNase digestion (RNase-free DNase Set; Qiagen). cDNA synthesis was performed using RevertAid (Fermentas) according to the manufacturer's instructions. Quantitative PCR was performed using an Mx3000P qPCR system (Agilent). Each assay was performed in triplicates. Amplification of St-*ABCG1* was performed with the Maxima Probe qPCR Master Mix (Fermentas) using Roche Universal Probe Library Probe #35 and the primers 5′-GGTCGCGATCCTAGCCTATT-3′ and 5′-ATCCTATCGCGATTGATGAAG-3′, amplification of the endogenous control St-*EF1α* using Roche Universal Probe Library Probe #162 and the primers 5′-CACTGCCCAGGTCATCATC-3′ and 5′-GTCGAGCACTGGTGCATATC-3′. Relative transcript levels were determined using the MxPro qPCR Software (Agilent).

Subcellular Localization of St-ABCG1 in *Arabidopsis* Protoplasts

The coding region of St-*ABCG1* was amplified without a stop codon and cloned into the vector *pUBC-DEST-RFP* (Grefen et al., 2010) to generate an *ABCG1-RFP* expression construct under the control of the *ubiquitin 10* promoter. As a control for plasma membrane localization, a construct encoding FLS2-YFP was used (*pXCSG-YFP-FLS2*; Feys et al., 2005; Robatzek et al., 2006).

Arabidopsis thaliana Columbia-0 plants were grown under controlled conditions in a phytochamber (8 h light/16 h dark at 20°C and 18°C, respectively). Isolation and transformation of protoplasts were performed as described (Yoo et al., 2007), with the aforementioned plasmids (10 μg DNA/100 μL protoplasts). Sixteen hours after transformation, microscopy was conducted with a confocal laser scanning microscope (LSM710, ZEN 2009 software; Carl Zeiss). For excitation of RFP and YFP, 561- and 514-nm lasers were used, respectively. Emission filter settings were 569 to 617 nm for RFP, 505 to 557 nm for YFP, and 643 to 721 nm for chlorophyll.

Cloning of St-*ABCG1* Full-Length cDNA, RNAi Constructs, and Generation of Transgenic Plants

The primers 5′-ATGTCAAGGATAGTGGCGGA-3′ and 5′-TCACCTTCTCTTGTTCTTACTTCCA-3′ were used to amplify a full-length cDNA of St-*ABCG1* from RNA of Pep-13-treated leaves.

To clone the *ABCG1*-RNAi fragment, primers (5′-TCGATTCGAGATTGTTGAAAG-3′ and 5′-GATTCGATAACTTGGCTGATG-3′) were designed from a potato EST (MICRO.15286.C1) and used to amplify a 413-bp fragment from potato cDNA. The *ABCG1*-RNAi RNAi fragment was cloned into *pENTR/D-TOPO* (Invitrogen) and transferred via LR recombination (Invitrogen) to *pHELLSGATE8* (Wesley et al., 2001). Potato plants (*S. tuberosum* cv Désirée) were transformed with *Agrobacterium tumefaciens* AGL0 (Lazo et al., 1991) containing the RNAi vectors. Transgenic plants were regenerated as described (Feltkamp et al., 1995).

Microscopy

Segments of roots and tubers of 3-month-old soil-grown plants from the greenhouse were fixed with 3% glutaraldehyde (Sigma-Aldrich) in 0.1 M sodium cacodylate buffer (SCB; Carl Roth), pH 7.2, for 4 h at room temperature, washed with SCB, and dehydrated in a graded ethanol series. Thereafter, the samples were stepwise infiltrated with Technovit

7100 (Heraeus-Kulzer), transferred into embedding molds, and finally polymerized in the absence of air at 4°C.

Semithin sections (3 μm) were stained with 1% toluidine blue and observed with an Axioskop 20 light microscope (Zeiss) or used for histochemical staining of suberin using fluorol yellow 088 (Sigma-Aldrich) as described (Brundrett et al., 1991). Sections were viewed using a confocal laser scanning microscope (LSM700, ZEN 2011 software; Carl Zeiss). Fluorol yellow-stained periderm sections or autofluorescence of unstained periderm were analyzed with an excitation wavelength of 405 nm for autofluorescence and 488 nm for fluorol yellow 088. Emission filter settings were 418 to 480 nm for autofluorescence and 520 to 588 nm for fluorol yellow 088.

Chemical Analyses of Tuber Periderm

Wild-type, empty vector, and *ABCG1*-RNAi (lines B4, F2, N, and P) plants were grown in parallel in a greenhouse. After 3 months, tubers of four plants per genotype were individually harvested, carefully rinsed with tap water to remove adhering soil, and stored for 1 week at 4°C in the dark before sampling. Two biological replicate experiments were performed on independent sets of plants grown at different times resulting in a total of 48 tuber pools [genotype (6) × individual plant (4) × biological replicate (2)].

Four uniform tubers of an individual pool were punched with a cork borer (diameter of 6 mm). From the resulting samples, the tuber skin was detached, the remaining parenchyma manually removed as completely as possible using a scalpel, and then shock frozen in liquid nitrogen. Four individual periderm disks per tuber were pooled, ground using a mortar and pestle, and stored at –80°C until extraction.

The remaining tubers of an individual pool were boiled for 10 to 15 min in water and peeled. The combined peels were digested at room temperature in a mixture of 2% (v/v) cellulase (from *Trichoderma reesei* ATCC 26921; Sigma-Aldrich) and 2% (v/v) pectinase (Trenolin Super DF; Erbsloeh) in 0.01 M citric acid (pH 3.0, adjusted with KOH) in the presence of 1 mM sodium azide (Schreiber et al., 2005). After 7 d, digested peels were thoroughly washed with deionized water, dried in a vacuum dessicator over calcium chloride until constant weight, and homogenized for 2 min at 30 Hz in a mixer mill (MM301; Retsch) using steel beads (diameter of 25 mm). For delipidation, homogenized peels were sonicated for 10 min at 50°C with methanol (2 × 5 mL), methanol/chloroform (2/1 [v/v]; 2 × 5 mL), and methanol/chloroform (1/2 [v/v]; 2 × 5 mL), dried in vacuo at 40°C, and stored until chemical depolymerization at room temperature.

For the extraction and analysis of semipolar metabolites, undigested periderm (50 ± 3 mg) was weighed into a precooled 2-mL polypropylene tube and 500 μL methanol/water, 8/2 (v/v), precooled at –28°C was added. While vortexing occasionally, the mixture was allowed to reach room temperature within 15 min. After addition of steel beads (diameter of 6 mm), the mixture was homogenized for three min at 30 Hz using a mixer mill (MM301; Retsch), sonicated for 15 min at 20°C, and centrifuged for 10 min at 16,000*g*. For the analysis of the major glycoalkaloids, a 20-μL aliquot of the supernatant was diluted with 580 μL methanol/water, 3/7 (v/v), centrifuged for 10 min at 16,000*g*, and subjected to UPLC/PDA/ESI(+)-QTOFMS. For the analysis of all other components, a 100-μL aliquot of the supernatant was diluted with 200 μL water, centrifuged for 10 min at 16,000*g*, and subjected to UPLC/PDA/ESI(+)-QTOFMS as well.

Target compounds were relatively quantified by integration of extracted ion chromatograms (*m/z*-width ± 0.02) using quantifier ions and retention times from Supplemental Table 11. The resulting peak areas were normalized to sample fresh weight and $\log_2$ transformed.

For the extraction and analysis of apolar metabolites, undigested periderm (50 ± 3 mg) was weighed into a precooled 2-mL polypropylene tube and 1000 μL methanol/methyl *tert*-butyl ether, 1/3 (v/v), precooled at –28°C was added. While vortexing occasionally, the mixture was allowed to reach room temperature within 15 min and subsequently homogenized for 3 min at 30 Hz using a mixer mill (MM301; Retsch) and a steel bead (diameter of 6 mm). After addition of 500 μL methanol/water, 1/3 (v/v), vortexing, and centrifugation for 4 min at 9000*g*, a 500-μL aliquot of the nonpolar (upper) phase was transferred into a new 2-mL polypropylene tube and evaporated to dryness at 40°C using a vacuum centrifuge. The remaining residue was thoroughly redissolved by sonication for 10 min at 20°C in 200 μL methanol. After centrifugation for 5 min at 16,000*g*, the supernatant was subjected to UPLC/PDA/ESI(-)-QTOFMS.

Target compounds were relatively quantified by integration of extracted ion chromatograms (*m/z*-width ± 0.02) using quantifier ions and retention times from Supplemental Tables 5 to 9 and 12 to 14. The resulting peak areas were normalized to sample fresh weight and $\log_2$ transformed.

To analyze suberin after chemical depolymerization, digested periderm (10 ± 2 mg) was weighed into a 2-mL polypropylene tube, and 1 mL boron trifluoride-methanol solution (10% [w/w]; Sigma-Aldrich) as well as the internal standards heptadecanoic acid (25 μg; Sigma-Aldrich), 15-hydroxypentadecanoic acid (25 μg; ABCR), and 1-pentadecanol (25 μg; Sigma-Aldrich) were added. The mixture was vigorously shaken for 24 h at 55°C using a thermomixer. Afterwards, the mixture was transferred into a 15-mL screw cap glass tube, quenched with 1 mL water, and extracted with a total of 4 mL chloroform. The combined chloroform extract was dried over sodium sulfate. For quantification of the major suberin components, a 1-mL aliquot of the chloroform extract was evaporated to dryness at 30°C using a vacuum centrifuge, derivatized with 40 μL anhydrous pyridine and 80 μL *N*,*O*-bis(trimethylsilyl)trifluoroacetamide (Macherey-Nagel) for 1 h at 40°C, and analyzed by gas chromatography/electron ionization-quantitative mass spectrometry (GC/EI-QMS) using a defined split ratio (split ratio 1:10). For quantification of the minor suberin components, a 2-mL aliquot of the chloroform extract was evaporated and derivatized as described above and analyzed by GC/EI-QMS after splitless injection.

Target compounds were relatively quantified by integration of extracted ion chromatograms using quantifier/qualifier ions and retention times from Supplemental Tables 1 to 4 and 15. The resulting peak areas were normalized to the peak area of the corresponding internal standard and sample dry weight.

UPLC/PDA/ESI-QTOFMS

Analysis of Polar Extracts

Chromatographic separations were performed at 40°C on an Acquity UPLC system (Waters) equipped with a HSS T3 column (100 × 1.0 mm, particle size 1.8 μm; Waters) applying the following binary gradient at a flow rate of 150 μL min^{-1}: 0 to 0.5 min, isocratic 99% A (water/formic acid, 99.9/0.1 [v/v]), 1% B (acetonitrile/formic acid, 99.9/0.1 [v/v]); 0.5 to 10 min, linear from 1 to 60% B; 10 to 12 min, isocratic 95% B. The injection volume was 2.3 μL (full loop injection). Eluting components were consecutively detected in a wavelength range of 200 to 500 nm using a photodiode array detector (Waters) and in a *m/z* range of 100 to 1000 using a micrOTOF-Q I hybrid quadrupole time-of-flight mass spectrometer (Bruker Daltonics) equipped with an Apollo II electrospray ion source in positive ion mode using following instrument settings: nebulizer gas, nitrogen, 1.6 bar; dry gas, nitrogen, 6 L/min, 190°C; capillary, 4000 V; end plate offset, −500 V; funnel 1 RF, 200 V; funnel 2 RF, 200 V; in-source CID energy, 0 V; hexapole RF, 100 V; quadrupole ion energy, 3 eV; collision gas, argon; collision energy, 3 eV; collision RF 200/350 V (timing 50/50); transfer time, 70 μs; prepulse storage, 5 μs; pulser frequency, 10 kHz; spectra rate, 3 Hz.

Analysis of Apolar Extracts

Chromatographic separations were performed at 40°C on an Acquity UPLC system equipped with a BEH C_8 column (100 × 1.0 mm, particle size 1.7 μm; Waters) applying the following binary gradient at a flow rate of

150 μL min^{-1}: 0 to 1 min, isocratic 50% A (water/formic acid, 99.9/0.1 [v/v]), 50% B (acetonitrile/formic acid, 99.9/0.1 [v/v]); 1 to 16 min, linear from 50 to 100% B; 16 to 22 min, isocratic 100% B. The injection volume was 2.3 μL (full loop injection). Eluting components were consecutively detected in a wavelength range of 200 to 500 nm using a photodiode array detector and in a *m/z* range of 90 to 1200 using a micrOTOF-Q I and following instrument settings: nebulizer gas, nitrogen, 1.6 bar; dry gas, nitrogen, 6 L/min, 190°C; capillary, 4000 V; end plate offset, −500 V; funnel 1 RF, 200 V; funnel 2 RF, 200 V; in-source CID energy, 0 V; hexapole RF, 100 V; quadrupole ion energy, 3 eV; collision gas, argon; collision energy, 10 eV; collision RF 200/400/600/800 V (timing 25/25/25/25); transfer time, 70 μs; prepulse storage, 5 μs; pulser frequency, 10 kHz; spectra rate, 3 Hz.

Mass spectra were acquired in centroid mode. Calibration of *m/z* was performed for individual raw data files on lithium formate cluster ions obtained by automatic infusion of 20 μL 10 mM lithium hydroxide in isopropanol/water/formic acid, 49.9/49.9/0.2 (v/v/v), at the end of the gradient using a diverter valve.

GC/EI-QMS

Gas chromatographic separation was performed on an Agilent 6890N GC equipped with a split/splitless inlet and a ZB-5 column (30 m × 0.25 mm, 0.25 μm 95% dimethyl/5% diphenyl polysiloxane film, 10 m integrated guard column; Phenomenex). Derivatized samples (1 μL) were injected applying an injector temperature of 310°C. Helium was used as carrier gas at a constant flow rate of 1 mL min^{-1} through the column. The purge time (splitless injection) was set to 1 min at a purge flow of 20 mL min^{-1}. After injection, the oven temperature was kept at 70°C for 1 min and subsequently raised to 200°C at 20°C min^{-1}. After a 2-min isothermal period at 200°C, the oven temperature was raised to 350°C at 9°C min^{-1} where it was held again for 2 min. Eluting components were detected after a solvent delay of 5.5 min using an Agilent 5975 Series Mass Selective Detector. The transfer line temperature was set at 350°C during the entire analysis. Electrospray ionization at 70 eV was employed at an ion source temperature of 230°C. Mass spectra were recorded from *m/z* 40 to 600 at a scan rate of 3 s^{-1}. The mass spectrometer was autotuned and mass calibrated according to the manufacturer's recommendations using perfluorotributylamine (FC-43).

Bioinformatic Analyses

Statistical analyses were performed using one-way and two-way ANOVA and Student's *t* test. Potato genome sequence comparisons were done at http://solgenomics.net/ and http://solanaceae.plantbiology.msu.edu/. Nucleotide and protein sequence comparisons were performed at http://www.ncbi.nlm.nih.gov/, and phylogenetic tree analysis was performed using MEGA4 (Tamura et al., 2007).

Accession Numbers

Sequence data from this article can be found in the GenBank/EMBL databases under the following accession numbers: St-ABCG1: XP_006345915, At-ABCG1: O80946.1, At-ABCG2: Q9ZUT0, At-ABCG3: Q9ZUU9, At-ABCG4: Q9SW08, At-ABCG5: Q9SIT6.1, At-ABCG6: Q9FNB5.1, At-ABCG7: Q9ZU35.1, At-ABCG8: Q9FLX5.1, At-ABCG9: Q9SZR9.2, At-ABCG10: Q9MAH4.1, At-ABCG11: Q8RXN0.1, At-ABCG12: Q9C8K2.1, At-ABCG13: Q9C8J8.1, At-ABCG14: Q9C6W5.1, At-ABCG15: Q8RWI9.2, At-ABCG16: Q9M2V7.2, At-ABCG17: Q9M2V6.1, At-ABCG18: Q9M2V5.1, At-ABCG19: Q9M3D6.1, At-ABCG20: Q9LFG8.1, At-ABCG21: Q7XA72.2, At-ABCG22: Q93YS4.1, At-ABCG23: Q3E9B8.1; At-ABCG24: Q9MAG3.2, At-ABCG25: Q84TH5.1, At-ABCG26: Q9LK50.2, At-ABCG27: Q9FT51.1, At-ABCG28: Q9FF46.1, At-ABCG29: Q94A18.2, At-ABCG30: Q8GZ52.2; At-ABCG31: Q7PC88.1, At-ABCG32: O81016.1, At-ABCG33: Q9ZUT8.1, At-ABCG34: Q7PC87.1, At-ABCG35: Q7PC86.1, At-ABCG36: Q9XIE2.1, At-ABCG37: Q9LFH0.1, At-ABCG38: Q7PC85.1, At-ABCG39: Q7PC84.1, At-ABCG40: Q9M9E1.1, At-ABCG41: Q7PC83.1, At-ABCG42: Q7PC82.1, and At-ABCG43: Q7PC81.1

Supplemental Data

The following materials are available in the online version of this article.

Supplemental Figure 1. Structure and Expression of St-*ABCG1*

Supplemental Figure 2. Evolutionary Relationships of St-ABCG1 and At-ABCG1 to 43.

Supplemental Figure 3. Reduced *ABCG1* Expression in *ABCG1*-RNAi Lines.

Supplemental Figure 4. Morphological Alterations in Tuber Periderm and Roots of *ABCG1*-RNAi Lines.

Supplemental Figure 5. Suberin Composition in Individual *ABCG1*-RNAi Lines.

Supplemental Figure 6. UV Chromatograms (324 nm) Obtained from Apolar Extracts of *ABCG1*-RNAi and Wild-Type Tuber Periderm.

Supplemental Figure 7. Putative Molecular Structures of Ferulic Acid Conjugates Detectable in Apolar Extracts of *ABCG1*-RNAi Tuber Periderm.

Supplemental Figure 8. Extracted Ion Chromatograms Corresponding to Deprotonated Molecular Ions of Feruloyloxy Docosanoic Acid and Feruloyloxy Docosanoyl Glycerol Obtained from Apolar Extracts of *ABCG1*-RNAi Tuber Periderm by UPLC/PDA/ESI(-)-QTOFMS.

Supplemental Table 1. Analytical Data of 1-Trimethylsilyloxy Alkanes Detected by GC/EI-QMS.

Supplemental Table 2. Analytical Data of α,ω-Dicarboxylic Acid Dimethyl Esters Detected by GC/EI-QMS.

Supplemental Table 3. Analytical Data of Fatty Acid Methyl Esters Detected by GC/EI-QMS.

Supplemental Table 4. Analytical Data of ω-Trimethylsilyloxy Fatty Acid Methyl Esters Detected by GC/EI-QMS.

Supplemental Table 5. Analytical Data of Feruloyloxy Fatty Acids Detected by UPLC/ESI(-)-QTOFMS.

Supplemental Table 6. Analytical Data of Feruloyloxy Fatty Acid Glycerol Esters Detected by UPLC/ESI(-)-QTOFMS.

Supplemental Table 7. Analytical Data of Alkyl Ferulates Detected by UPLC/ESI(-)-QTOFMS.

Supplemental Table 8. Analytical Data of Hydroxyalkyl Ferulates Detected by UPLC/ESI(-)-QTOFMS.

Supplemental Table 9. Analytical Data of Feruloyloxyalkyl Ferulates Detected by UPLC/ESI(-)-QTOFMS.

Supplemental Table 10. Relative Quantification of Ferulic Acid Conjugates, ω-Hydroxy Fatty Acids, α,ω-Dicarboxylic Acids, and Fatty Acids in Apolar Extracts of *ABCG1*-RNAi and Control Periderm.

Supplemental Table 11. Analytical Data of Aromatic Amino Acids, Phenylpropanoids, Anthocyanins, and Glycoalkaloids Detected by UPLC/ESI(+)-QTOFMS.

Supplemental Table 12. Analytical Data of ω-Hydroxy Fatty Acids Detected by UPLC/ESI(-)-QTOFMS.

Supplemental Table 13. Analytical Data of α,ω-Dicarboxylic Acids Detected by UPLC/ESI(-)-QTOFMS.

Supplemental Table 14. Analytical Data of Fatty Acids Detected by UPLC/ESI(-)-QTOFMS.

Supplemental Table 15. Analytical Data of Trimethylsilyloxycinnamic Acid Methyl Esters Detected by GC/EI-QMS.

Supplemental Data Set 1. Text File of the Alignment Used for the Phylogenetic Analysis of ABCG Proteins in Supplemental Figure 2.

ACKNOWLEDGMENTS

We thank Felix Mauch (University of Fribourg, Switzerland) for the *P. infestans* isolate CRA208m and Silke Robatzek (John Innes Center, Norwich, UK) for *pXCSG-YFP-FLS2*. We thank Kirstin and Ivo Feussner (University of Göttingen) for providing standards for GC-MS analyses. This work was supported by the Deutsche Forschungsgemeinschaft (SFB648 TPA4 and TPZ1).

AUTHOR CONTRIBUTIONS

R.L., S.A., L.E.-L., M.S., S.S., N.S., G.H., B.W., and C.B. designed and performed experiments and analyzed data. U.S. and N.F. performed experiments. D.S. and C.B. contributed new analytic tools. C.B. and L.E.-L. wrote the article. S.R. designed the research and wrote the article.

Received February 28, 2014; revised July 4, 2014; accepted July 16, 2014; published August 8, 2014.

REFERENCES

Beisson, F., Li, Y., Bonaventure, G., Pollard, M., and Ohlrogge, J.B. (2007). The acyltransferase GPAT5 is required for the synthesis of suberin in seed coat and root of Arabidopsis. Plant Cell **19:** 351–368.

Beisson, F., Li-Beisson, Y., and Pollard, M. (2012). Solving the puzzles of cutin and suberin polymer biosynthesis. Curr. Opin. Plant Biol. **15:** 329–337.

Benveniste, I., Tijet, N., Adas, F., Philipps, G., Salaün, J.P., and Durst, F. (1998). CYP86A1 from *Arabidopsis thaliana* encodes a cytochrome P450-dependent fatty acid omega-hydroxylase. Biochem. Biophys. Res. Commun. **243:** 688–693.

Bessire, M., Borel, S., Fabre, G., Carraça, L., Efremova, N., Yephremov, A., Cao, Y., Jetter, R., Jacquat, A.C., Métraux, J.P., and Nawrath, C. (2011). A member of the PLEIOTROPIC DRUG RESISTANCE family of ATP binding cassette transporters is required for the formation of a functional cuticle in Arabidopsis. Plant Cell **23:** 1958–1970.

Bird, D., Beisson, F., Brigham, A., Shin, J., Greer, S., Jetter, R., Kunst, L., Wu, X., Yephremov, A., and Samuels, L. (2007). Characterization of Arabidopsis ABCG11/WBC11, an ATP binding cassette (ABC) transporter that is required for cuticular lipid secretion. Plant J. **52:** 485–498.

Brundrett, M.C., Kendrick, B., and Peterson, C.A. (1991). Efficient lipid staining in plant material with sudan red 7B or fluorol [correction of fluoral] yellow 088 in polyethylene glycol-glycerol. Biotech. Histochem. **66:** 111–116.

Brunner, F., Rosahl, S., Lee, J., Rudd, J.J., Geiler, C., Kauppinen, S., Rasmussen, G., Scheel, D., and Nürnberger, T. (2002). Pep-13, a plant defense-inducing pathogen-associated pattern from *Phytophthora* transglutaminases. EMBO J. **21:** 6681–6688.

Domergue, F., Vishwanath, S.J., Joubès, J., Ono, J., Lee, J.A., Bourdon, M., Alhattab, R., Lowe, C., Pascal, S., Lessire, R., and Rowland, O. (2010). Three Arabidopsis fatty acyl-coenzyme A reductases, FAR1, FAR4, and FAR5, generate primary fatty alcohols associated with suberin deposition. Plant Physiol. **153:** 1539–1554.

Feltkamp, D., Baumann, E., Schmalenbach, W., Masterson, R., and Rosahl, S. (1995). Expression of the mannopine synthase promoter in roots is dependent on the *mas* elements and correlates with high transcript levels of *mas*-binding factor. Plant Sci. **109:** 57–65.

Feys, B.J., Wiermer, M., Bhat, R.A., Moisan, L.J., Medina-Escobar, N., Neu, C., Cabral, A., and Parker, J.E. (2005). Arabidopsis SENESCENCE-ASSOCIATED GENE101 stabilizes and signals within an ENHANCED DISEASE SUSCEPTIBILITY1 complex in plant innate immunity. Plant Cell **17:** 2601–2613.

Franke, R., Höfer, R., Briesen, I., Emsermann, M., Efremova, N., Yephremov, A., and Schreiber, L. (2009). The DAISY gene from Arabidopsis encodes a fatty acid elongase condensing enzyme involved in the biosynthesis of aliphatic suberin in roots and the chalaza-micropyle region of seeds. Plant J. **57:** 80–95.

Franke, R., and Schreiber, L. (2007). Suberin—a biopolyester forming apoplastic plant interfaces. Curr. Opin. Plant Biol. **10:** 252–259.

Fry, W. (2008). *Phytophthora infestans*: the plant (and *R* gene) destroyer. Mol. Plant Pathol. **9:** 385–402.

Grefen, C., Donald, N., Hashimoto, K., Kudla, J., Schumacher, K., and Blatt, M.R. (2010). A ubiquitin-10 promoter-based vector set for fluorescent protein tagging facilitates temporal stability and native protein distribution in transient and stable expression studies. Plant J. **64:** 355–365.

Halim, V.A., Hunger, A., Macioszek, V., Landgraf, P., Nürnberger, T., Scheel, D., and Rosahl, S. (2004). The oligopeptide elicitor Pep-13 induces salicylic acid-dependent and -independent defense reactions in potato. Physiol. Mol. Plant Pathol. **64:** 311–318.

Halim, V.A., Altmann, S., Ellinger, D., Eschen-Lippold, L., Miersch, O., Scheel, D., and Rosahl, S. (2009). PAMP-induced defense responses in potato require both salicylic acid and jasmonic acid. Plant J. **57:** 230–242.

Höfer, R., Briesen, I., Beck, M., Pinot, F., Schreiber, L., and Franke, R. (2008). The Arabidopsis cytochrome P450 CYP86A1 encodes a fatty acid omega-hydroxylase involved in suberin monomer biosynthesis. J. Exp. Bot. **59:** 2347–2360.

Kloosterman, B., et al. (2008). Genes driving potato tuber initiation and growth: identification based on transcriptional changes using the POCI array. Funct. Integr. Genomics **8:** 329–340.

Lazo, G.R., Stein, P.A., and Ludwig, R.A. (1991). A DNA transformation-competent Arabidopsis genomic library in Agrobacterium. Biotechnology (N. Y.) **9:** 963–967.

Li, Y., Beisson, F., Ohlrogge, J., and Pollard, M. (2007a). Monoacylglycerols are components of root waxes and can be produced in the aerial cuticle by ectopic expression of a suberin-associated acyltransferase. Plant Physiol. **144:** 1267–1277.

Li, Y., Beisson, F., Koo, A.J.K., Molina, I., Pollard, M., and Ohlrogge, J. (2007b). Identification of acyltransferases required for cutin biosynthesis and production of cutin with suberin-like monomers. Proc. Natl. Acad. Sci. USA **104:** 18339–18344.

Molina, I., Li-Beisson, Y., Beisson, F., Ohlrogge, J.B., and Pollard, M. (2009). Identification of an Arabidopsis feruloyl-coenzyme A transferase required for suberin synthesis. Plant Physiol. **151:** 1317–1328.

Panikashvili, D., Shi, J.X., Schreiber, L., and Aharoni, A. (2011). The Arabidopsis ABCG13 transporter is required for flower cuticle secretion and patterning of the petal epidermis. New Phytol. **190:** 113–124.

Panikashvili, D., Shi, J.X., Bocobza, S., Franke, R.B., Schreiber, L., and Aharoni, A. (2010). The Arabidopsis DSO/ABCG11 transporter affects cutin metabolism in reproductive organs and suberin in roots. Mol. Plant **3:** 563–575.

Pighin, J.A., Zheng, H., Balakshin, L.J., Goodman, I.P., Western, T.L., Jetter, R., Kunst, L., and Samuels, A.L. (2004). Plant cuticular lipid export requires an ABC transporter. Science **306:** 702–704.

Pollard, M., Beisson, F., Li, Y., and Ohlrogge, J.B. (2008). Building lipid barriers: biosynthesis of cutin and suberin. Trends Plant Sci. **13:** 236–246.

Ranathunge, K., Schreiber, L., and Franke, R. (2011). Suberin research in the genomics era—new interest for an old polymer. Plant Sci. **180:** 399–413.

Robatzek, S., Chinchilla, D., and Boller, T. (2006). Ligand-induced endocytosis of the pattern recognition receptor FLS2 in Arabidopsis. Genes Dev. **20:** 537–542.

Schreiber, L., Franke, R., and Hartmann, K. (2005). Wax and suberin development of native and wound periderm of potato (*Solanum tuberosum* L.) and its relation to peridermal transpiration. Planta **220:** 520–530.

Serra, O., Hohn, C., Franke, R., Prat, S., Molinas, M., and Figueras, M. (2010). A feruloyl transferase involved in the biosynthesis of suberin and suberin-associated wax is required for maturation and sealing properties of potato periderm. Plant J. **62:** 277–290.

Serra, O., Soler, M., Hohn, C., Franke, R., Schreiber, L., Prat, S., Molinas, M., and Figueras, M. (2009a). Silencing of StKCS6 in potato periderm leads to reduced chain lengths of suberin and wax compounds and increased peridermal transpiration. J. Exp. Bot. **60:** 697–707.

Serra, O., Soler, M., Hohn, C., Sauveplane, V., Pinot, F., Franke, R., Schreiber, L., Prat, S., Molinas, M., and Figueras, M. (2009b). CYP86A33-targeted gene silencing in potato tuber alters suberin composition, distorts suberin lamellae, and impairs the periderm's water barrier function. Plant Physiol. **149:** 1050–1060.

Tamura, K., Dudley, J., Nei, M., and Kumar, S. (2007). MEGA4: molecular evolutionary genetics analysis (MEGA) software version 4.0. Mol. Biol. Evol. **24:** 1596–1599.

Wesley, S.V., et al. (2001). Construct design for efficient, effective and high-throughput gene silencing in plants. Plant J. **27:** 581–590.

Xu, X., et al; Potato Genome Sequencing Consortium (2011). Genome sequence and analysis of the tuber crop potato. Nature **475:** 189–195.

Yang, W., Pollard, M., Li-Beisson, Y., Beisson, F., Feig, M., and Ohlrogge, J. (2010). A distinct type of glycerol-3-phosphate acyltransferase with sn-2 preference and phosphatase activity producing 2-monoacylglycerol. Proc. Natl. Acad. Sci. USA **107:** 12040–12045.

Yeats, T.H., Martin, L.B., Viart, H.M., Isaacson, T., He, Y., Zhao, L., Matas, A.J., Buda, G.J., Domozych, D.S., Clausen, M.H., and Rose, J.K. (2012). The identification of cutin synthase: formation of the plant polyester cutin. Nat. Chem. Biol. **8:** 609–611.

Yoo, S.-D., Cho, Y.-H., and Sheen, J. (2007). Arabidopsis mesophyll protoplasts: a versatile cell system for transient gene expression analysis. Nat. Protoc. **2:** 1565–1572.